Available online at www.sciencedirect.com

ScienceDirect

Computers & Fluids 36 (2007) 667–679

computers & fluids

www.elsevier.com/locate/compfluid

A finite element method for the solution of rotary pumps

Guillaume Houzeaux *, Ramon Codina

International Center for Numerical Methods in Engineering (CIMNE), Edificio C1, Campus Nord UPC, Gran Capità s/n, 08034 Barcelona, Spain

Received 26 December 2004; received in revised form 18 October 2005; accepted 10 February 2006
Available online 4 October 2006

Abstract

We present in this paper a numerical strategy for the simulation of rotary positive displacement pumps, taking as an example a gear pump. While the two gears of the pump are rotating, the intersection between them changes in time. Therefore, the computational domain should be recomputed in some way at each time step. The strategy used here consists in dividing a cycle into a certain number of time steps and obtaining different computational meshes for each of these time steps. The coupling between two consecutive time steps is achieved by interpolating the flow unknowns in a proper way. This geometrical decomposition enables one to have a plain control over the mesh, particularly in the zones of interest, which are the gap between the gears and the casing, and the engagement and disengagement zones of the gears.

1. Introduction

Volk [1]: "Simply stated, a pump is a machine used to move liquid through a piping system, and to raise the pressure of the liquid".

In this paper, we define a possible strategy to simulate the flow in rotary pumps of positive displacement type. Our work is based on the study of a particular pump, belonging to the family of gear pumps: an external gear pump. However, the analysis framework is applicable to the whole family.

The gear pump we consider is sketched in Fig. 1, each gear having $N_{\text{teeth}} = 11$ teeth. The pump works as follows. The shaft of one of the gears is driven by a motor: this is the driving gear. It engages around the other one, called the driven gear. When the teeth of the two gears start disengaging (near the center of the pump), the consequent low pressure sucks in the fluid. Upon further rotation, the fluid is trapped in between the space formed by this cavity and the casing. The fluid is then carried around towards the discharge side of the pump. As in principle it cannot flow back through the very "small gap" between the teeth and the casing and neither through the engaged teeth of the gears, it is entirely ejected to the outport. Therefore, unlike a fan (for example), the flow rate is expected not to depend on the pressure difference between the inlet and outlet. At high pressures however, some fluid may slip through the gap and along the casing walls from the discharge side (high pressure) to the suction side (low pressure). Thus the efficiency of the pump may be affected. It is also well known that for a higher viscous fluid, the leakage will be smaller, but it requires more power to provide the same rotational speed.

If we assume that all the fluid trapped between the teeth is delivered to the outport (no leakage), the volume flow rate Q (mm^3/s) provided by the pump is directly proportional to the velocity of rotation ω (rad/s) of the gears. The constant of proportionally is called the volumetric constant and is referred to as C_v (mm^3/rad)

$$Q = C_v \omega.$$

The units considered along this work are mm, s and kg.

The gear pumps have many applications. In the car industry, they are used to pump oil towards the elements

* Corresponding author. Tel.: +34 934016485; fax: +34 934016517.
E-mail addresses: houzeaux@cimne.upc.edu (G. Houzeaux), ramon.codina@upc.edu (R. Codina).
URLs: http://www.cimne.com/cfdgroup (G. Houzeaux), http://www.cimne.com/cfdgroup (R. Codina).

0045-7930/$ - see front matter © 2006 Elsevier Ltd. All rights reserved.
doi:10.1016/j.compfluid.2006.02.005

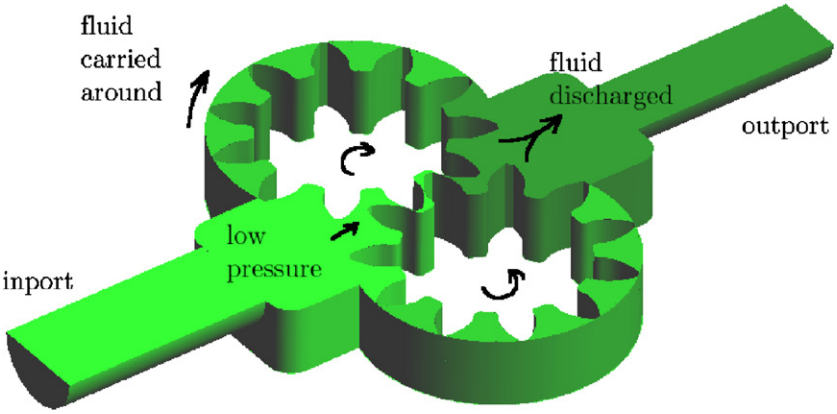

Fig. 1. External gear pump (only half part).

to be lubricated; in construction equipment they work as a hydraulic power unit (e.g. excavator); they deliver gas in petrol stations, since the flow rate delivered is directly proportional to the velocity of rotation of the gears; they can serve as a counter (e.g. for metering water consumption) for they are reversible and can therefore be engaged by the flow of fluid; they are used as hydraulic pumps in snow plows, etc.

The main goal of this study consists in estimating the pressure distribution within the suction side to avoid cavitation. Cavitation is mainly due to the vaporization of the oil or to the presence of air in it. Vaporization occurs when the pressure is too low or the temperature too high. Low pressure can occur for two main reasons. The first reason is an unsufficient inlet pressure (in our case the atmospheric pressure if the tank is at the same level). If this is the case, the depression needed to suck in the fluid and overcome the pressure looses from the tank can be propitious to the onset of vaporization. The second reason could be the presence of a highly swirling flow, which characteristic high velocities are accompanied by low pressures. Cavitation affects the pumping capability of the pump as the gear cavities are not filled completely with oil. Actually the scenario is worse, as once cavitation has occurred, a subsequent increase of pressure provokes the collapses of the vapor bubbles. The resulting compression waves contribute to the erosion of the structure and the generation of high level noise.

The study of cavitation is not addressed in this study. But the numerical simulations will allow us to detect the zones where the pressure is more likely to fall below the vapor pressure of the fluid. This study will help therefore to orient the modification to carry out on the original geometry to improve the efficiency of the pump.

The study of the gear pump is organized as follows. We first explain how to treat the geometrical issues. In particular, we discuss the possible geometrical modifications which enable one to simplify the numerical study of the problem. We then present the governing equations of the flow, that is the Navier–Stokes equations and their associated boundary conditions. In the next section, some numerical aspects are explained, including the space and time discretizations as well as the algorithm used to treat the evolving configuration of the pump. In the final section, numerical results are presented. We want to compare the results obtained for two possible treatments of the geometry and those obtained for two and three-dimensional simulations.

2. Geometrical and meshing aspects

2.1. Gap between teeth and casing

The section through the symmetry plane of the pump is shown in Fig. 2, for a given time step. As noted in Section 1, the suction and discharge sides of the pump are only

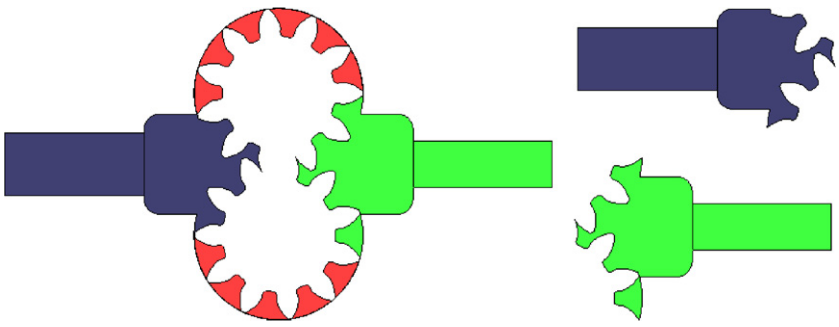

Fig. 2. Section at symmetry plane. (Left) Gap between gears and casing is considered: suction and discharge chambers are connected. (Right) No gap: suction and discharge chambers are independent.

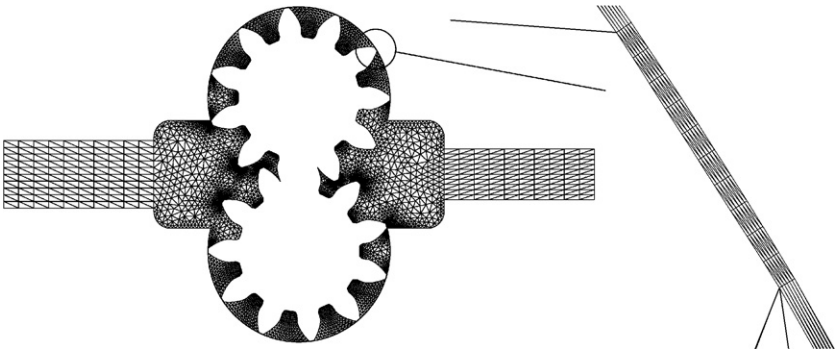

Fig. 3. Mesh of the configuration shown in Fig. 2. (Left) Whole mesh. (Right) Structured mesh in the gap.

connected if a gap is present. The right part of the figure illustrates this possible independency. On the one hand, if the gap is not considered, then both sides can be treated separately. On the other hand, if the effects of pressure loads are important, the leakage must be taken into account and therefore the whole pump must be treated. If this is the case, the corresponding mesh will of course be much denser than in the first situation. Fig. 3 shows an example of structured mesh in the gap and unstructured mesh in the rest of the domain. This mesh enables the accurate solution of the inport, the outport and the gap between the gears and the casing.

2.2. Gear intersection

In a gear pump, only one gear is driven by a motor, the second being driven by the first one. They are therefore in close contact and while they are turning around, their common intersection changes in time. Thus the computational domain should be recomputed in some way at each time step of the simulation. In [2], the authors use a fictitious domain method to solve a lobe pump, which exhibits the same geometrical difficulty as the gear pump we have in hands. In the fictitious domain method, the positions of the lobes are identified by turning on and turning off the elements that are in the fluid and inside the lobes, respectively, at each time step. The boundary condition on the lobe boundaries are imposed in a weak way by introducing a Lagrange multiplier. In [3], the authors use an Arbitrary Lagrangian Eulerian (ALE) method [4,5] to follow the rotation of the gears of a lobe and a gear pumps. However, the automatic remeshing technique they adopt does not enable a perfect control on the mesh, which can be uncircumventable if one wants to accurately solve the gap and the intersection of the gears. The method chosen in this work to solve these deficiencies is based on an ALE formulation with fixed meshes (FMALE), in the sense that the evolving geometry is not meshed in an automatic way (like in classical ALE with remeshing) but a priori, before starting the simulation. It is similar to the method used in [6].

We first notice that the same geometrical configuration is repeated periodically. This period correspond to the time between two tooth passings. Let us define a configuration cycle the period to recover the same configuration of the pump. For a gear pump with gears of N_{teeth} teeth, the duration of a configuration cycle is $2\pi/(\omega N_{\text{teeth}})$. The FMALE method applied to this context consists in dividing a configuration cycle into a given number of time steps. The coupling between two consecutive time steps will be explained in Section 4. Fig. 4 shows the geometries that could be obtained at four consecutive time steps.

2.3. Half pump

We mentioned in the first section that in some cases, the gap between the gears and the casing might be neglected. This greatly simplifies the computation as the inport and outport can be treated independently. By applying the strategy introduced previously in Section 2.2, we can therefore obtain different meshes for a configuration cycle of the inport only. This can be achieved by attaching the teeth to the casing (with subsequent error in flow rate). Fig. 5 shows the geometries that could be obtained at four consecutive time steps, considering only the suction side of the pump.

3. Problem statement

3.1. The Navier–Stokes equations

Let Ω be an open bounded domain of $\mathbb{R}^2$ or $\mathbb{R}^3$. Consider the time interval $(0,T)$. Define ρ as the density of the fluid and μ as its viscosity. The governing equations are the transient Navier–Stokes (NS) equations for the velocity $\boldsymbol{u}$ and the mechanical (not thermodynamic) pressure p

$$\rho\partial_t\boldsymbol{u} + \rho(\boldsymbol{u}_a\cdot\nabla)\boldsymbol{u} - 2\mu\nabla\cdot\boldsymbol{\varepsilon}(\boldsymbol{u}) + \nabla p = \boldsymbol{0} \quad \text{in } \Omega\times(0,T),$$
$$\nabla\cdot\boldsymbol{u} = 0 \quad \text{in } \Omega\times(0,T),$$

where $\boldsymbol{\varepsilon}(\boldsymbol{u})$ is the rate of deformation tensor given by

$$\boldsymbol{\varepsilon}(\boldsymbol{u}) = \frac{1}{2}(\nabla\boldsymbol{u} + \nabla\boldsymbol{u}^t).$$

We note that the advection velocity of the momentum equation has been corrected from $\boldsymbol{u}$ to $\boldsymbol{u}_a$ since in the method proposed here the domain Ω is changing with time; this point will be treated in Section 4.

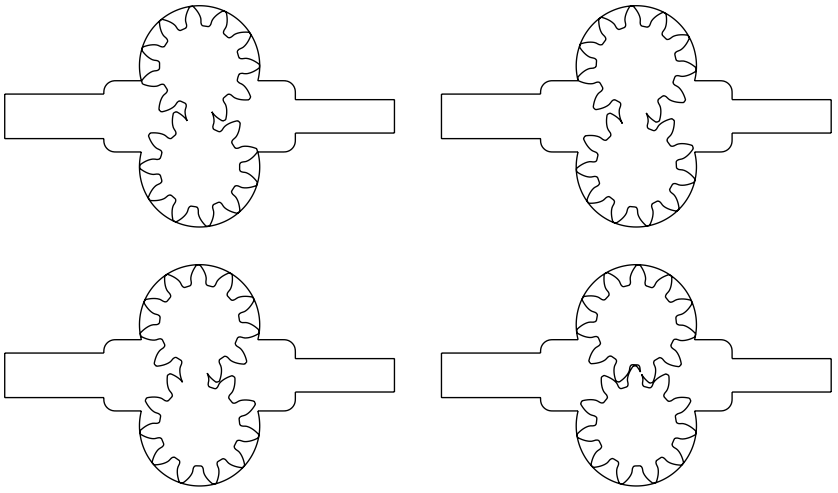

Fig. 4. Whole-pump. Geometries at consecutive time steps.

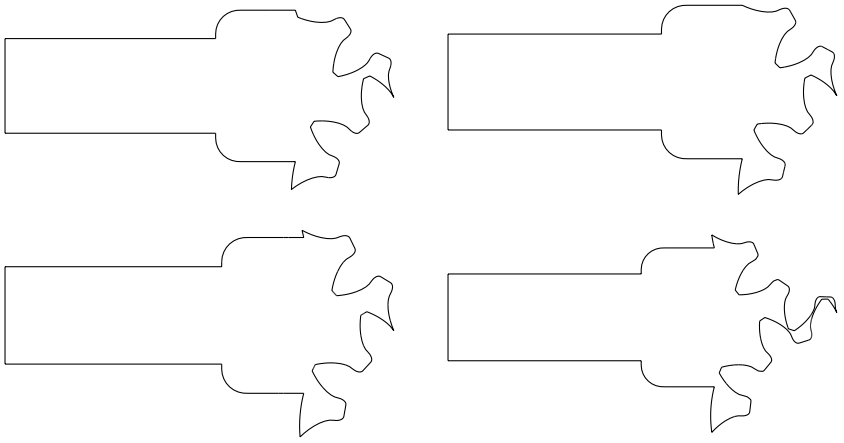

Fig. 5. Half-pump. Geometries at consecutive time steps.

The authors would like to point out that turbulence modeling is not envisaged in the framework of this paper. However, all the cases presented in Section 5 have also been performed using a turbulence model, namely the Spalart–Allmaras one-equation model [7]. As no turbulent effects were noticeable, the authors preferred not to consider them in order to clarify the exposition.

3.2. Boundary conditions

The Navier–Stokes equations must be supplied with boundary and initial conditions. The initial condition is only needed for the velocity, we denote it by $\boldsymbol{u}_0$. As for the boundary conditions, let us divide the boundary of Ω as $\partial\Omega = \Gamma_{\mathrm{D}} \cup \Gamma_{\mathrm{N}}$, where D holds for Dirichlet and N holds for Neumann. We consider here the following two conditions of Dirichlet and Neumann types:

$$\boldsymbol{u} = \boldsymbol{u}_{\mathrm{D}} \quad \text{on } \Gamma_{\mathrm{D}} \times (0,T),$$
$$\boldsymbol{\sigma}\cdot\boldsymbol{n} = \boldsymbol{t}_{\mathrm{N}} \quad \text{on } \Gamma_{\mathrm{N}} \times (0,T),$$

where $\boldsymbol{n}$ is the outward unit normal to $\partial\Omega$, and $\boldsymbol{\sigma}$ is the stress tensor given by

$$\boldsymbol{\sigma} = -p\boldsymbol{I} + 2\mu\boldsymbol{\varepsilon}(\boldsymbol{u}),$$

$\boldsymbol{I}$ being the two(three)-dimensional identity. We have chosen as Neumann condition the prescription of the traction $\boldsymbol{\sigma}\cdot n$ because it enters naturally the variational form of the problem (only the diffusion term is integrated by parts). Let us observe that for uniform flows we have that $\boldsymbol{\varepsilon}(\boldsymbol{u}) = \boldsymbol{0}$, and that for high Reynolds number flows the viscous term of the traction can be neglected so that

$$\boldsymbol{\sigma}\cdot\boldsymbol{n} = -p\boldsymbol{n} \quad \text{for uniform flows,}$$
$$\boldsymbol{\sigma}\cdot\boldsymbol{n} \approx -p\boldsymbol{n} \quad \text{for high Reynolds number flows.}$$

We will see that for the particular operating conditions of this pump, the prescription of the traction approximates very well that of the pressure.

4. Numerical strategy

In the previous section we presented the governing equations of the flow. However, some purely numerical and algorithmic ingredients are necessary to solve the flow in time. We first introduce the finite element method and

the time discretization which are considered to solve the partial differential equations. Finally we present the strategy for the coupling of the different configurations defined for each time step.

4.1. Finite element method and time discretization

4.1.1. Space discretization

The NS equations are solved using a Finite Element model based on a stabilized Galerkin method. It is well-known that the Galerkin formulation can lack stability for two major reasons. The first reason is related to the compatibility of the finite element spaces for the velocity and the pressure which have to satisfy the so-called Ladyzhenskaya–Brezzi–Babuška (LBB) condition. This condition is necessary to obtain a stability estimate for the pressure; without requiring this condition, the pressure would be out of control. The second reason is attributed to the relative importance of the viscous and convective effects in the momentum equation. The stabilized formulation is based on the algebraic variational subgrid scale (SGS) model first introduced in [8]. The variational SGS model first argues that the inability of the mesh to resolve all the flow scales is responsible for the numerical instabilities. Therefore, the model calculates in some approximate way the unresolved scales of the flow, i.e. the scales smaller than the mesh size. The method is extensively described in [9]. In this work, we consider only one type of element using equal order interpolation for the velocity and the pressure, that is the P1/P1 element, continuous and linear in velocity and pressure. This element does not satisfy the LBB condition and therefore requires the use of the SGS stabilization.

4.1.2. Time discretization

The time discretization is carried out using the generalized trapezoidal rule, i.e. a finite difference scheme. To do so, we consider a partition $0 = t^0 < t^1 < \cdots < t^{N_{\text{time}}} = T$ of the time interval $(0, T)$ of interest. The time step is denoted as $\delta t = t^n - t^{n-1}$ and is constant for $n = 1,\ldots, N_{\text{time}}$. The backward Euler scheme is considered here. The solution of the equations is therefore implicit and unconditionally stable. Given an initial condition $\boldsymbol{u}^0$, the backward Euler scheme consists in solving for each $n = 1,\ldots, N_{\text{time}}$

$$\begin{aligned} &\rho\frac{\boldsymbol{u}^n - \boldsymbol{u}^{n-1}}{\delta t} + \rho(\boldsymbol{u}_a^n \cdot \nabla)\boldsymbol{u}^n - 2\mu\nabla\cdot\boldsymbol{\varepsilon}(\boldsymbol{u}^n) + \nabla p^n = \boldsymbol{0} \quad \text{in } \Omega, \\ &\nabla\cdot\boldsymbol{u}^n = 0 \quad \text{in } \Omega \end{aligned} \tag{1}$$

with appropriate boundary conditions.

4.2. Coupling of the configurations

As mentioned in Section 2.2, the main difficulty of solving the pump is the treatment of the zones of engagement and disengagement of the teeth. A possible solution consists in defining a new geometry and a new mesh at each time step of the numerical simulation, the position of the gears being known a priori. Then the flow equations are solved successively on each geometry to obtain $(\boldsymbol{u}^n, p^n)$, by taking as a previous time step solution $\boldsymbol{u}^{n-1}$ the interpolated variables obtained on the previous geometry.

In fact, we can take advantage of the numerical strategy based on an *implicit* solution of the Navier–Stokes equations for which we can afford relatively large time steps. In addition, by using the backward Euler time integration scheme, which is unconditionally stable for fixed meshes, we can expect the resulting numerical strategy to be stable. In order to choose the time step we have to make a compromise which, as always, faces accuracy with computation time. On the one hand, the time step must be large enough so that we do not have to calculate too many geometries and to generate too many meshes. On the other hand, the time step must be small enough to capture the important time scales of the flow. We assume that the leading period of the flow will be that of a tooth passing and that we can neglect the effect of smaller scales on the mean flow. According to these considerations, we decide to solve N_{conf} times the flow equations during a configuration cycle (between two tooth passings) with N_{conf} close to 10 (10 being approximately the number of points to solve with sufficient accuracy a sine type signal). Therefore we set

$$\delta t = \frac{2\pi}{\omega N_{\text{teeth}} N_{\text{conf}}}.$$

We have N_{conf} configurations per cycle, each one with an associated mesh. The question is how do we have to couple the solutions obtained on the meshes. As shown in Fig. 6, some nodes of the mesh of a given configuration can be located inside the gear of the previous configuration. Therefore we have to take into account in some way the mesh movement from one configuration to the next one. Let us first introduce some definitions.

We define a *host element* of a point of coordinates $\boldsymbol{x}$ in a mesh j as the element where the point is located. Let us define a *hosted node* as a node having a host element, and a *lost node* a node without host element, which is the case when a node falls inside a gear (see [10] for the element search strategy). Let us identify with a subscript i the variables considered in mesh i, so that $\boldsymbol{u}_i^n$ is the velocity obtained on configuration i, referred to as Ω_i, at time step n. Note that n and i are related through the equation

$$i = n - \text{int}\left(\frac{n}{N_{\text{conf}}}\right) N_{\text{conf}}.$$

The procedure to construct the interpolation operator $I^{i,j}$ from mesh j to mesh i is the following:

For each configuration $i = 1,\ldots, N_{\text{conf}}$ **do**
  If $i = 1$ **then**
    Set $j = N_{\text{conf}}$.
  Else

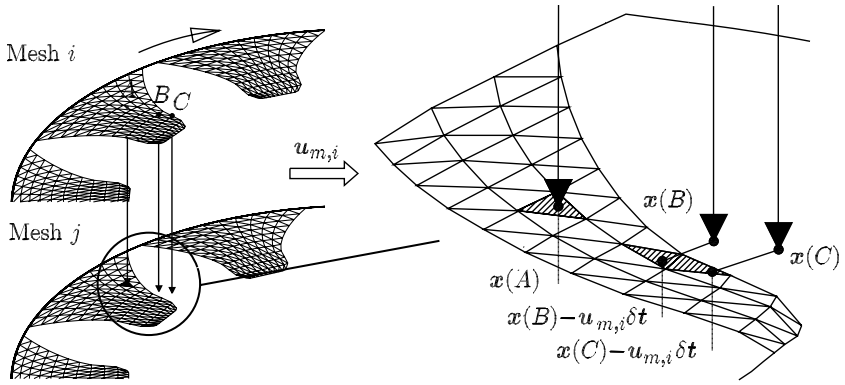

Fig. 6. Mesh velocity used for interpolation between consecutive meshes.

Set $j = i - 1$.
Endif
Look for the host elements of all nodes of i in mesh j.
Compute mesh velocity by solving e.g. Laplace's equation for $\boldsymbol{u}_{m,i}$
$\Delta \boldsymbol{u}_{m,i} = 0$,
with $\boldsymbol{u}_{m,i} = \boldsymbol{0}$ on hosted nodes,
and $\boldsymbol{u}_{m,i}$ = gear velocity for nodes on gear boundaries (4) and (5).
Find the host elements for the lost nodes in mesh j
with coordinates $\boldsymbol{x} - \boldsymbol{u}_{m,i}\delta t$.
Construct the interpolation operator $I^{i,j}$
using the classical Lagrange interpolation functions.
Return

Note that the previous configuration of the first configuration is configuration N_{conf}.

We now know how to interpolate a variable from one mesh to the next one. In the case of the Navier–Stokes equations, the only variable to interpolate is the velocity (note that for incompressible flows the time derivative of the pressure does not appear). When solving configuration i at time n, we must take in Eq. $(1)_1$ as solution of the previous time step $\boldsymbol{u}_i^{n-1}$ the following interpolated value:

$$\boldsymbol{u}_i^{n-1} = I^{i,j}(\boldsymbol{u}_j^{n-1}). \tag{2}$$

where $j = N_{\text{conf}}$ if $i = 1$ and $j = i - 1$ otherwise. Also, as the mesh is moving, we have to take into account the mesh velocity in the convective term of the NS equations, so that

$$\boldsymbol{u}_{a,i}^n = \boldsymbol{u}_i^n - \boldsymbol{u}_{m,i}.$$

The Navier–Stokes equations for configuration i at time n consists therefore in finding in domain Ω_i

$$\begin{aligned} &\rho \frac{\boldsymbol{u}_i^n - I^{i,j}(\boldsymbol{u}_j^{n-1})}{\delta t} + \rho[(\boldsymbol{u}_i^n - \boldsymbol{u}_{m,i}) \cdot \nabla]\boldsymbol{u}_i^n \\ &\quad - 2\mu \nabla \cdot \boldsymbol{\varepsilon}(\boldsymbol{u}_i^n) + \nabla p_i^n = \boldsymbol{0}, \\ &\nabla \cdot \boldsymbol{u}_i^n = 0. \end{aligned} \tag{3}$$

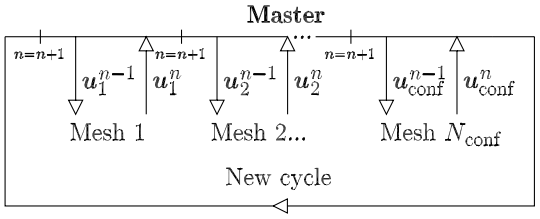

Fig. 7. Master–slave strategy to couple the meshes.

The coupling algorithm is the following:

Set $\boldsymbol{u}_{N_{\text{conf}}}^0$
Set $n = 0$
Set $\delta t = 2\pi/[\omega N_{\text{teeth}} N_{\text{conf}}]$
For each cycle $m = 1, \ldots, N_{\text{cycle}}$ **do**
  for each configuration $i = 1, \ldots, N_{\text{conf}}$ **do**
    Set $n = n + 1$
    If $i = 1$ **then**
      Set $j = N_{\text{conf}}$.
    Else
      Set $j = i - 1$.
    Endif
    Interpolate $\boldsymbol{u}_i^{n-1} = I^{i,j}(\boldsymbol{u}_j^{n-1})$
    Solve NS equation (3) for $(\boldsymbol{u}_i^n, p_i^n)$.
  Return
Return

This coupling is carried out using a master–slave strategy, as sketched in Fig. 7. The master code is in charge of the communication and of the interpolation between consecutive meshes, by performing the operation given by Eq. (2). The slaves are the N_{conf} processes corresponding to the N_{conf} meshes of the Navier–Stokes solver. The master code uses the Message Passing Interface standard (MPI) [11] to establish the communication and synchronization of the processes.

5. Results

This section presents some numerical results. In the first part we demonstrate the convergence properties of the

coupling strategy through the solution of a simple test example. The following sections treat with the case of interest, that is the gear pump. Some complementary information can be found in the web page referenced in [12].

5.1. Test problem

Through the solution of a simple test problem we want to check the convergence of the solution with the number of configurations N_{conf}. The transient solutions will be compared to a stationary solution. Fig. 8(Left) shows the geometry used to solve the stationary problem. It consists of a fixed circular domain of radius 10 centered at the origin, and a unit square located at $(1,0)$ which is rotating with an angular velocity $\boldsymbol{\omega} = [0,0,\omega]^t$, $\omega = 2\pi$. The problem is solved in a non-inertial frame of reference with angular velocity $\boldsymbol{\omega}$, in which the velocity of the square is zero, and that of the circle $-\boldsymbol{\omega}\times\boldsymbol{x}$. We work without dimensions and set $\rho = 1$, $\mu = 1$. In order to perform the convergence test, three cases are considered: 4, 10 and 20 configurations. These configurations are shown in Fig. 8. All the meshes have approximately 2300 P1/P1 elements. It is expected that the solution gets better as the number of configurations increases.

To check this, we have plotted the evolution of the velocity module at point Q with coordinates $(2,0)$ for the four cases. In the case of the stationary solution, the velocity at point Q should be computed as $\boldsymbol{u} + \boldsymbol{\omega}\times\boldsymbol{x}$ (in order to take into account the rotation of the frame of reference) at the points located at $(2\cos(\omega t), -2\sin(\omega t))$. Fig. 9(Left) compares the results for the four simulations. After a short transient period, the three transient simulations attain the expected periodic behavior. The figure confirms that the solution is getting better as the number of configurations increases. We even note that only the 20 configurations simulation is able to capture the sudden velocity decrease, just before the square reaches its initial position. Fig. 9(Right) compares the velocity module obtained on a horizontal cut passing through the origin, and enables to draw the same conclusions.

5.2. Data of the problem

We now go on with the gear pump. The properties of the oil we are considering are

$$\mu = 3.0\times10^{-5}\ \text{kg/mm s},$$
$$\rho = 9.0\times10^{-7}\ \text{kg/mm}^3.$$

The pump works at 1500 rpm, which corresponds to angular velocities

$$\boldsymbol{\omega}_{\text{t}} = -[0,0,\omega]^t \quad \text{for the top gear},$$
$$\boldsymbol{\omega}_{\text{b}} = [0,0,\omega]^t \quad \text{for the bottom gear}$$

with

$$\omega = 157.08\ \text{rad/s}.$$

The center of the top and bottom gears are located at $\boldsymbol{x}_{\text{t}}$ and $\boldsymbol{x}_{\text{b}}$, respectively. The velocities on the teeth are thus

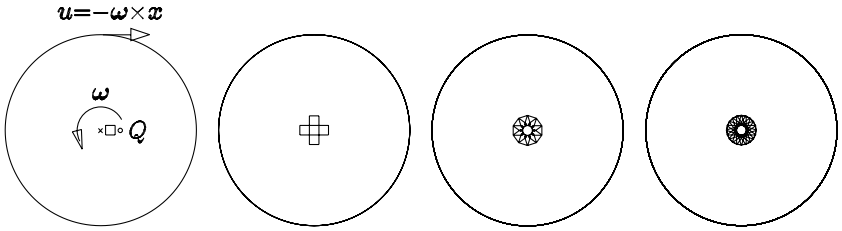

Fig. 8. Test problem. From left to right: 1 configuration for stationary solution with boundary conditions; 4 configurations; 10 configurations; 20 configurations.

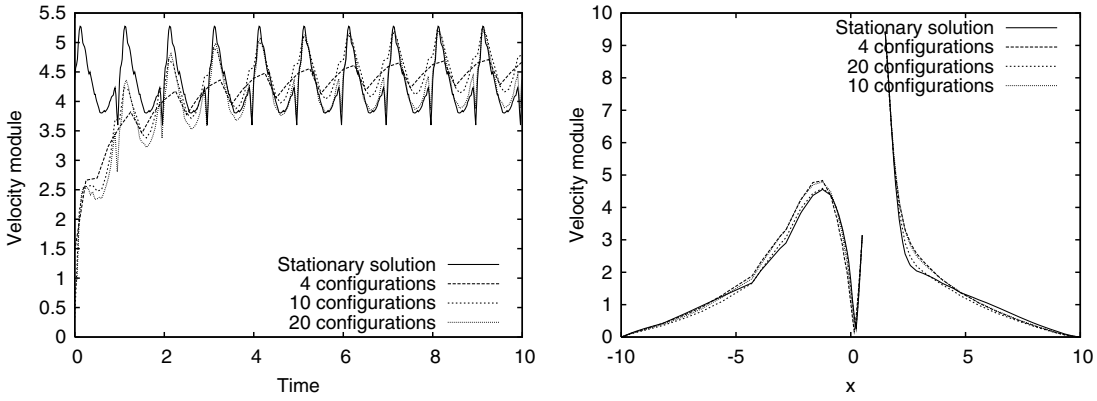

Fig. 9. Test problem. (Left) Evolution of the velocity module at point Q. (Right) Velocity module along a horizontal cut passing through the origin.

prescribed to the velocities of their corresponding gears, that is

$$\boldsymbol{u} = \boldsymbol{\omega}_{\mathrm{t}} \times (\boldsymbol{x} - \boldsymbol{x}_{\mathrm{t}}) \quad \text{on the top gear,} \tag{4}$$

$$\boldsymbol{u} = \boldsymbol{\omega}_{\mathrm{b}} \times (\boldsymbol{x} - \boldsymbol{x}_{\mathrm{b}}) \quad \text{on the bottom gear,} \tag{5}$$

where $\boldsymbol{x}$ is the coordinate vector. On the casing, the velocity is $\boldsymbol{u} = \boldsymbol{0}$. The pump discharges an almost constant flow rate at constant velocity of rotation but has no control on the global pressure rise. The amount of pressure is controlled by the workload imposed on it. The pressure is prescribed by specifying the traction as

$$\boldsymbol{\sigma} \cdot \boldsymbol{n} = -p_{\mathrm{a}} \boldsymbol{n} \quad \text{at inport,}$$

$$\boldsymbol{\sigma} \cdot \boldsymbol{n} = -p_{\mathrm{o}} \boldsymbol{n} \quad \text{at outport.}$$

The boundary conditions are sketched in Fig. 10.

5.3. Two-dimensional pump

We present in this section the results obtained on the section at the symmetry plane of the pump. In particular, we compare the results obtained on the whole pump with those obtained by simulating only the suction side of the pump. We also investigate the effects of the gap.

5.3.1. Whole pump

We first consider the transient simulation of the whole pump. The pressure at the outport is fixed to a value p_{o} of 10 bars. At the inport, the pressure is that of the reservoir, i.e. the atmospheric pressure p_{a}, so that we have in our unit system:

$$p_{\mathrm{a}} = 10^2 \text{ kg/mm s}^2,$$

$$p_{\mathrm{o}} = 10^3 \text{ kg/mm s}^2,$$

which gives a pressure drop of $\Delta p = 900$ kg/mm s^2 = 9 bars. This prescribed pressure drop is the highest one studied in this paper. When studying the effects of the gap in Section 5.3.3, smaller pressure drops will be considered.

The configuration cycle is divided into $N_{\mathrm{conf}} = 10$ configurations, of which the four first ones are shown in Fig. 4. The time step of the simulation (which will be the same for all the numerical example) is therefore $\delta t \approx 3.64 \times 10^{-4}$. The meshes of the configurations are composed of 9738, 9780, 9563, 11,459, 12,297, 9569, 9668, 9220, 9500 and 9912 P1/P1 elements. The mesh of the first configuration is shown in Fig. 3.

Fig. 11 shows the evolution of the velocity module and pressure at points Q and R, as depicted in Fig. 10. We observe that a periodic solution is obtained after very few configuration cycles. The results that are presented from now on were obtained once the periodic flow was achieved.

The results obtained on the four first configurations are shown in Fig. 12. We can observe the high acceleration of the oil when the teeth disengage, especially for the fourth configuration.

Finally, Fig. 13 shows the pressure distribution along the casing of the first configuration, P being the reference point depicted in Fig. 10. We note that the pressure goes from its inlet value P_{a} to its outlet value p_{o} in stairway steps along the casing. We conclude that in this particular case, the prescription is almost that of the pressure. We also observe that almost all the pressure drop is achieved along the spaces between the teeth and the casing, that is the gap.

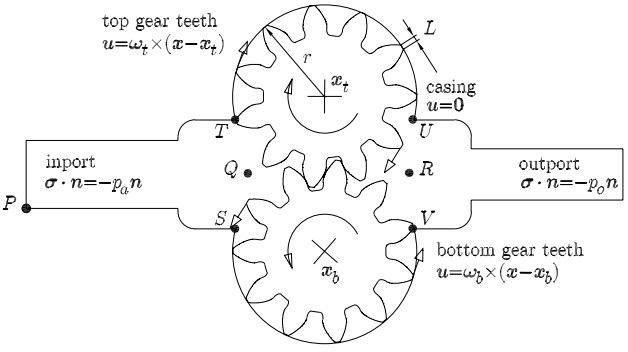

Fig. 10. Whole pump. Geometry and boundary conditions.

5.3.2. Half pump

We compare the solutions obtained on the whole pump configurations with that obtained on the half pump configuration, as shown in Figs. 4 and 5, respectively. The same pressure boundary conditions as those used for the whole

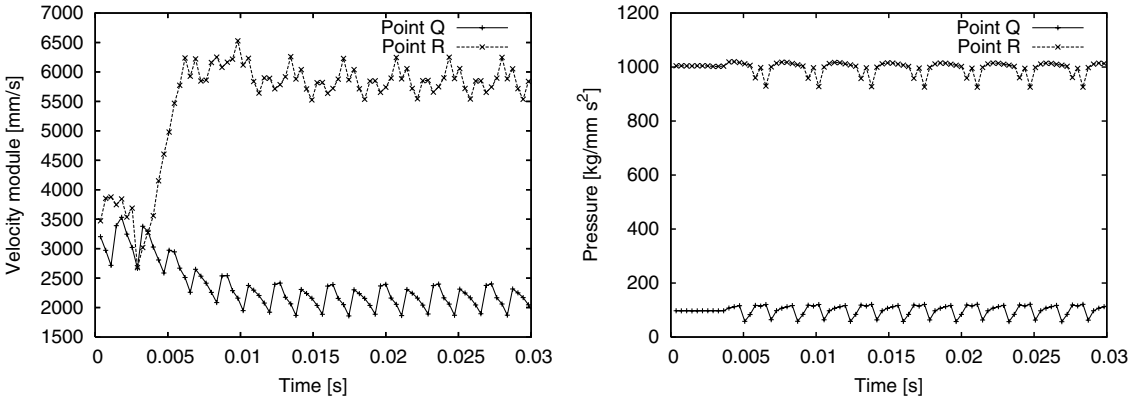

Fig. 11. Whole pump, $\Delta p = 900$ kg/mm s^2. Evolution of the solution at points Q and R. (Left) Velocity module. (Right) Pressure.

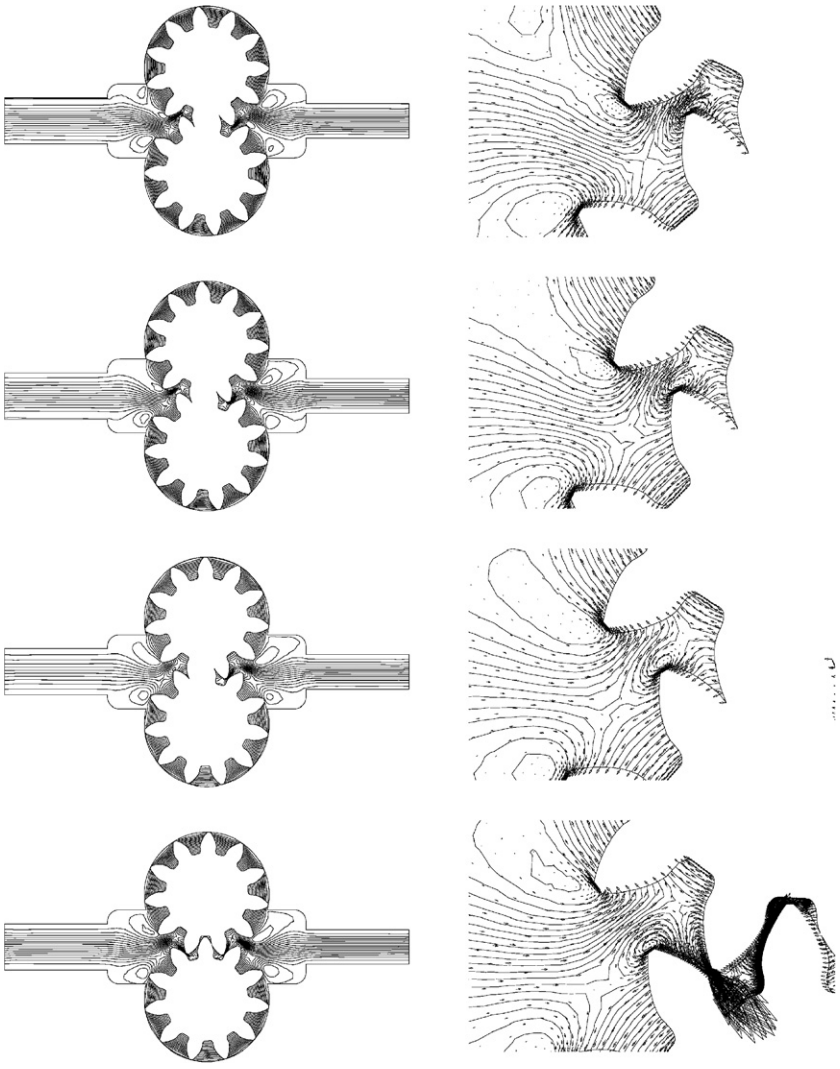

Fig. 12. Whole pump, $\Delta p = 900$ kg/mm s^2. Results of the first four configurations. (Left) Streamlines. (Right) Streamlines and velocity vectors in the disengagement zone.

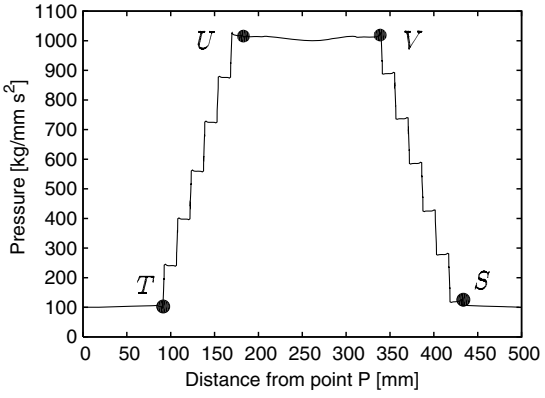

Fig. 13. Whole pump, $\Delta p = 900$ kg/mm s^2. Pressure distribution along the casing wall, from point P in the clockwise direction.

pump simulation are imposed. Thus, we are going to compare the results of the half pump with those obtained on the whole pump for the maximum pressure drop. This time, as only the suction chamber is solved, the meshes are much less dens. The ten configuration meshes are composed of 2039, 1733, 1757, 3600, 3351, 2114, 1741, 1751, 2133 and 2246 P1/P1 elements.

Fig. 14 shows the results obtained on the first configuration. We observe some relatively small differences between the half and whole pump results. In particular, the reverse flow of the gap stretches the recirculation zones of the suction sides towards the center.

Finally, Fig. 15 shows the evolution of the velocity module and pressure at point Q. We observe very similar values.

5.3.3. Effects of the gap

We now study more in detail the effect of the gap. To do so, we consider four values of p_o, that is 100, 400, 600 and 1000, which lead to pressure drops of $\Delta p = 0$, 300, 500 and 900, respectively. With these simulations we want to analyze the flow through the gap between a tooth and the casing. We consider the azimuthal component of the

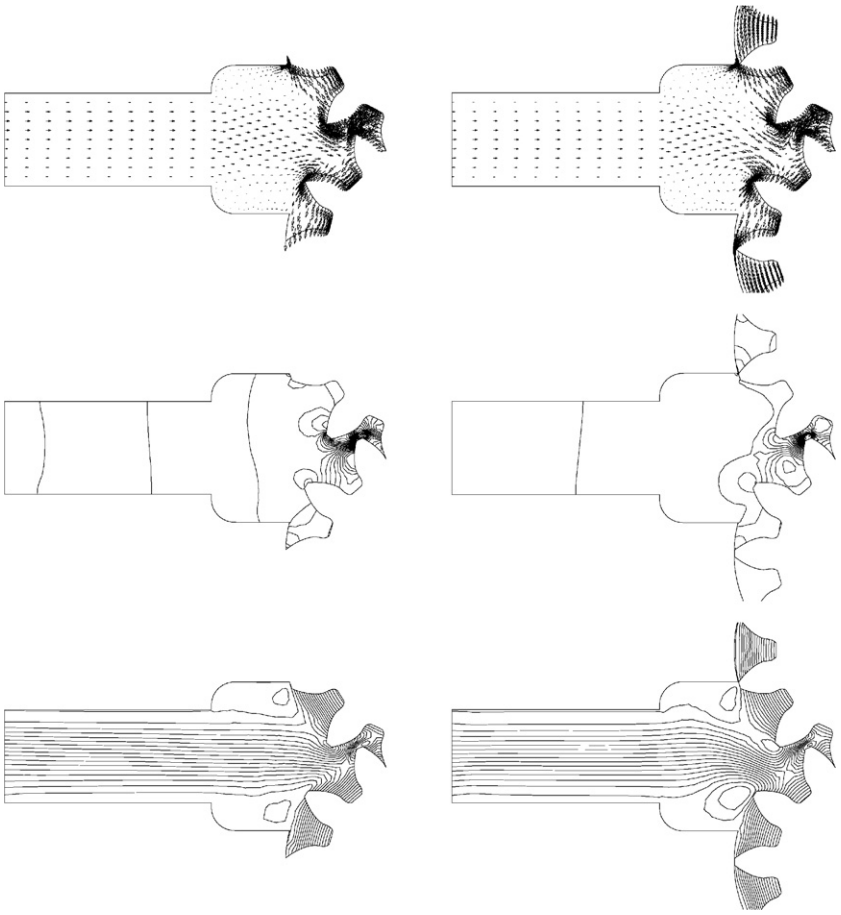

Fig. 14. Half and whole pumps, $\Delta p = 900$ kg/mm s^2. Results for the first configuration. (Left) Half pump. (Right) Whole pump. (Top) Velocity. (Mid) Pressure. (Bottom) Streamlines.

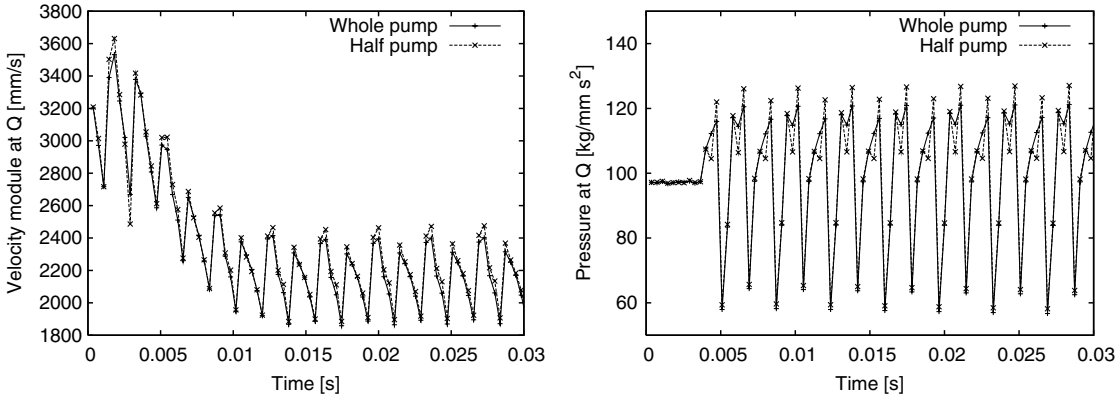

Fig. 15. Half and whole pumps, $\Delta p = 900$ kg/mm s^2. Evolution of the solution at point Q. (Left) Velocity module. (Right) Pressure.

velocity along a line passing through the gap of length $2H = 0.095$ mm. The external radius $r = 26.92$ mm of the gear being large and therefore the curvature being small, the flow in the gap can be approximated to a planar Couette flow. Let x be the streamwise direction and y be the crosswise direction and assume the flow is fully developed in x. See Fig. 16(Left).

Solving the Navier–Stokes equations in Cartesian coordinates for the velocity $\boldsymbol{u} = [u, v]^t$, we have that $u = u(y)$, $v = 0$ and

$$\mu \frac{\mathrm{d}^2 u}{\mathrm{d}y^2} = \frac{\mathrm{d}p}{\mathrm{d}x}.$$

We solve this equations with boundary conditions $u(-H) = U = \omega r$ and $u(H) = 0$ for a constant pressure gradient. The solution is

$$u = \frac{1}{2}\left(\frac{1}{\mu}\frac{\mathrm{d}p}{\mathrm{d}x}y^2 - \frac{U}{H}y + U - \frac{1}{\mu}\frac{\mathrm{d}p}{\mathrm{d}x}H^2\right). \tag{6}$$

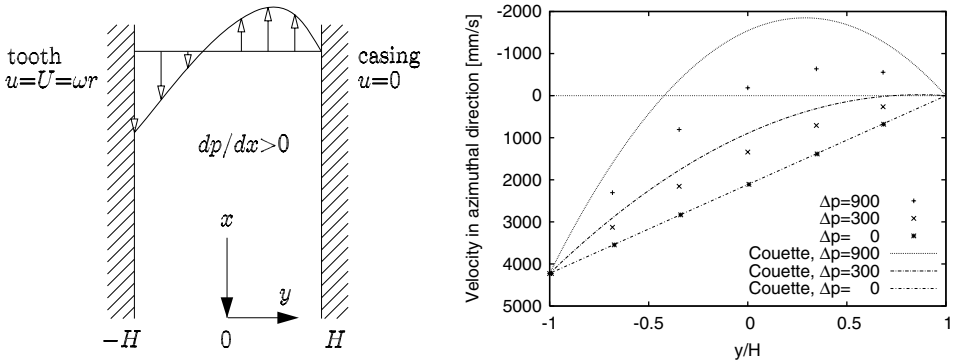

Fig. 16. Planar Couette flow comparisons. (Left) Geometry of the gap. (Right) Velocity in gap.

With positive pressure gradient, we expect the flow to be retarded. We remarked previously that almost all the pressure drop was achieved in the space between the gear and the casing. Therefore we assume that the imposed pressure gradient is entirely distributed over the "contact" zones of the gear with the casing. Let L be the length of these contact zones. We have $L = 1.44$ mm. We note that for the geometry considered there are six contact zones. We then approximate the pressure gradient as

$$\frac{\mathrm{d}p}{\mathrm{d}x} = \frac{p_\mathrm{o} - p_\mathrm{a}}{6L}. \tag{7}$$

From the solution obtained at different pressure drops, we pick up the velocity in the azimuthal direction at the centerline of the gap of an arbitrary tooth for the first configuration of the cycle, shown in Fig. 4(Top left). Fig. 16 shows the simulation results together with the planar Couette solution given by Eq. (6) with the pressure gradient given by Eq. (7). We observe that despite all the approximations we have stated (curvature neglected, fully developed flow assumed, pressure drop distributed in six equal parts), the flow in the gap follows the planar Couette flow solution. We have thus in hand a tool to approximate the leakage.

Fig. 17 shows the volume flow rate variation as a function of the pressure drop between inport and outport. The figure compares three results:

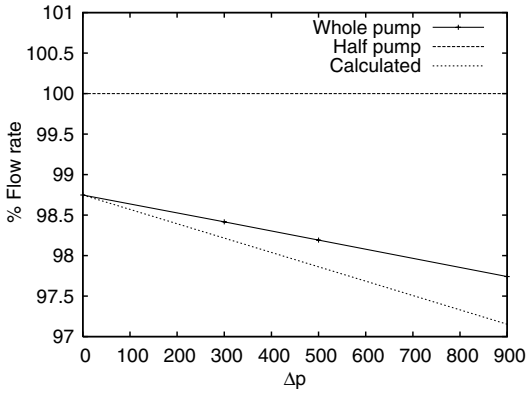

Fig. 17. Flow rate variation as a function of the pressure drop.

(1) Half pump: the flow rate obtained on half of the pump (the suction side) for which no reverse flow exists. This flow rate is used to normalize the two others.
(2) Whole pump: the flow rate computed on the whole pump for different pressure drops.
(3) Calculated: the flow rate obtained on the whole pump at zero pressure drop $Q(\mathrm{d}p/\mathrm{d}x = 0)$ minus the flow due to the Couette profile in the gap (at top and bottom gears) and given by

$$Q = Q(\mathrm{d}p/\mathrm{d}x = 0) - \frac{4}{3\mu}\frac{p_\mathrm{o} - p_\mathrm{a}}{6L}H^3.$$

Note that the flow rate obtained on the half pump is somewhat overestimated. This is due to the fact that when the half pump configurations were calculated, the teeth was extended to the casing to close the contact.

5.4. Three-dimensional pump

This section presents the results of the three-dimensional suction chamber, for which we neglect the effects of the gap. The meshes for the 10 configurations have 32,427, 54,145, 54,761, 37,782, 41,058, 42,472, 35,978, 38,811, 36,211 and 41,586 P1/P1 elements. The mesh of the first configuration is shown in Fig. 18(Left), while the right part of the figure shows a detail of the mesh near the teeth.

Fig. 19 compares the evolution of the velocity module and pressure at point Q with the results obtained on the two-dimensional half pump. In the three-dimensional pump, point Q is located at the same planar position than that of the two-dimensional pump on the symmetry plane. As expected, we observe that the velocity module is higher in the three-dimensional case. In fact, the flow rate is multiplied by the height of the pump with respect to that of the two-dimensional pump, while the entrance pipe is, in comparison, much smaller. If $U_{2\mathrm{D}}$ is the average inlet velocity, the flow rate in two dimensions would be $U_{2\mathrm{D}}dH$, d being the inlet diameter and H the pump height, whereas in three dimensions it would be $U_{3\mathrm{D}}\pi(d/2)^2$. Thus, the ratio of average inlet velocities is $U_{2\mathrm{D}}/U_{3\mathrm{D}} = d\pi/4H$,

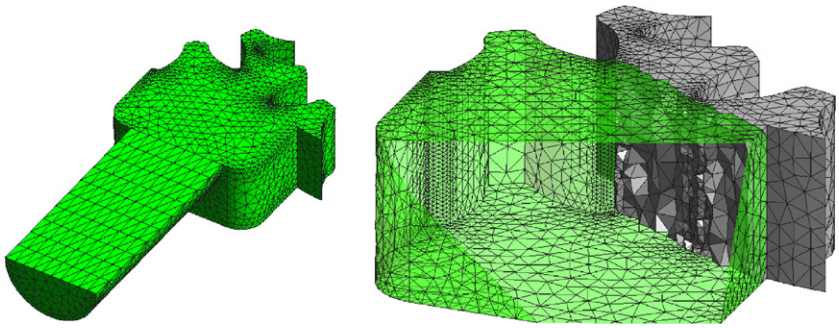

Fig. 18. Whole 3D pump. (Left) Mesh of the first configuration. (Right) Detail of the mesh near the teeth.

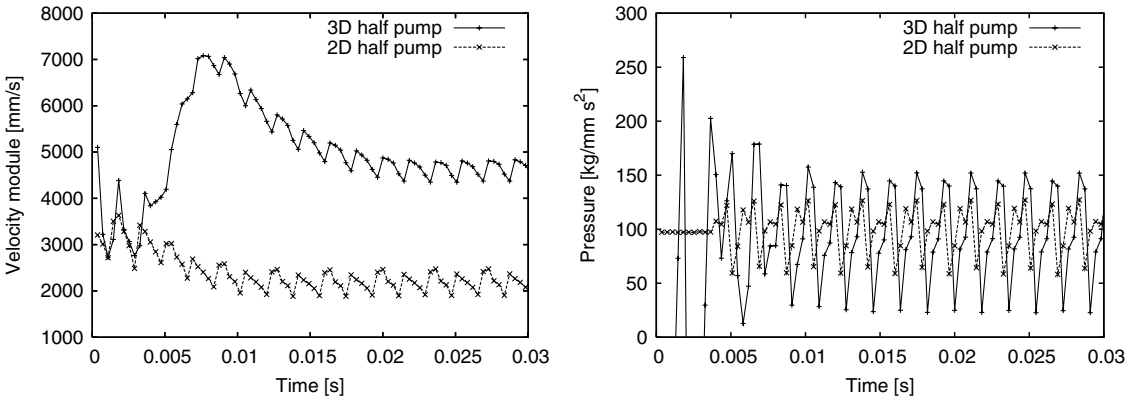

Fig. 19. 3D half and 2D half pumps. Evolution of the solution at point Q. (Left) Velocity module. (Right) Pressure.

that for the geometry we use yields $U_{2D}/U_{3D} = 0.54$. Note that the ratio estimated from Fig. 19 for the velocities at point Q is very close to this figure. Referring to this figure, we also note that contrary to the velocity, the pressure exhibits a quite similar evolution in both the two and three-dimensional cases.

Fig. 20 presents the velocity vectors and pressure contours of the first four configurations.

In Fig. 21, the particle path as well as the pressure on the boundary of the domain are shown. We can observe the three-dimensional vortex generated at the entrance of suction chamber.

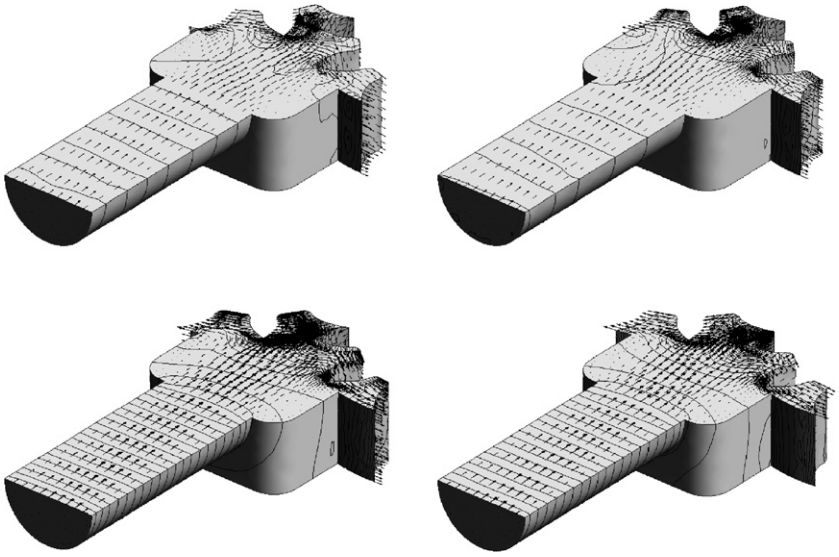

Fig. 20. Whole 3D pump. Velocity vectors and pressure contours of the first four configurations.

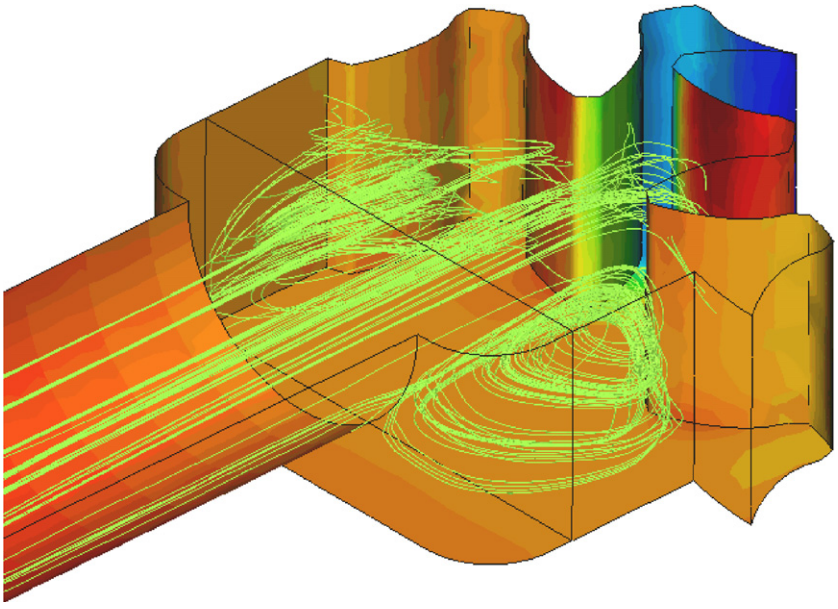

Fig. 21. Whole 3D pump. First configuration, pressure and particle path.

6. Conclusions

We have presented in this paper a finite element method to simulate the flow in rotary displacement pumps. The methodology consists in dividing the periodic geometrical cycle of the pump in a series of configurations, on which the transient Navier–Stokes equations are solved. Theses configurations are coupled with each other through a master–slave strategy. The numerical results have demonstrated the possibilities of the method.

With respect to other methods, we pretend that the present one enables on to accurately solve the leakage effects through the gap and the gear intersection. However, the authors would like to point out two drawbacks of the method. Firstly, the generations of the configurations can be quite tedious, if the geometry happens to be complicated. Secondly, one Navier–Stokes solver must solve each one of the configuration flow. Therefore, the memory required by the simulation can be quite large if many configurations are used. However, this can be circumvented if one uses MPI to distribute the calculation on many computers.

Acknowledgements

The work presented in this report was carried out in the framework of the GROWTH project of the European Union, GDR1-1999-10343, from January 2000 to January 2003, and entitled "Enhanced design and manufacturing of mini-hydraulic products (MINIHAP)". The authors would like to thank Marc Poy and Roberto Castilla from the Universitat Politècnica de Catalunya for providing the geometry of the pump and the experimental operating values and physical properties.

References

[1] Volk M. Pump characteristics and applications. Marcel Dekker, Inc.; 1996.
[2] Voorde JV, Vierendeels J, Dick E. Flow simulations in rotary volumetric pumps and compressors with the fictitious domain method. J Comput Appl Math 2004;168:491–9.
[3] Riemslagh K, Vierendeels J, Dick E. An arbitrary Lagrangian–Eulerian finite-volume method for the simulation of rotary displacement pump flow. Appl Numer Math 2000;32:419–33.
[4] Hughes TJ, Liu W, Zimmerman T. Lagrangian–Eulerian finite element formulation for incompressible viscous flows. CMAME 1981;29:329–49.
[5] Huerta A, Liu W. Viscous flow with large free surface motion. Comput Meth Appl Mech Eng 1988;69:277–324.
[6] Houzeaux G, Codina R. A finite element model for the simulation of lost foam casting. Int J Numer Meth Fluids 2004;46:203–26.
[7] Spalart P, Allmaras S. A one-equation turbulence model for aerodynamic flows. AIAA Paper 92-0439, 1992.
[8] Hughes TJ. Multiscale phenomena: Green's functions, the Dirichlet-to-Neumann formulation, subgrid scale models, bubbles and the origins of stabilized methods. Comput Meth Appl Mech Eng 1995; 127:387–401.
[9] Codina R. A stabilized finite element method for generalized stationary incompressible flows. Comput Meth Appl Mech Eng 2001;190: 2681–706.
[10] Houzeaux G, Codina R. A Chimera method based on a Dirichlet/Neumann (Robin) coupling for the Navier–Stokes equations. Comput Meth Appl Mech Eng 2003;192:3343–77.
[11] The message passing interface (MPI) standard. URL: http://www.unix.mcs.anl.gov/mpi/.
[12] Houzeaux G, Codina R. A finite element method for the solution of rotary displacement pumps: simulation results of a gear-pump. URL: http://www.cimne.com/cfdgroup/gear-pump.asp.